

Comments on the dispersion relation method to vector–vector interaction

R. Molina^{1,2,*}, L. S. Geng³, and E. Oset⁴

¹*Universidad Complutense de Madrid, Facultad de Físicas, Departamento de Física Teórica II, Plaza Ciencias, 1, 28040, Madrid*

²*Institute of Physics of the University of Sao Paulo, Rua do Matão 1371, Butantã, São Paulo, SP 05508-090, Brazil*

³*School of Physics and Nuclear Energy Engineering & International Research Center for Nuclei and Particles in the Cosmos & Beijing Key Laboratory of Advanced Nuclear Materials and Physics, Beihang University, Beijing 100191, China*

⁴*Departamento de Física Teórica and IFIC, Centro Mixto Universidad de Valencia-CSIC, Institutos de Investigación de Paterna, Aptdo. 22085, 46071 Valencia, Spain*

*E-mail: ramolinape@gmail.com

Received March 17, 2019; Revised August 6, 2019; Accepted August 20, 2019; Published October 21, 2019

.....
We study in detail the method proposed recently to study the vector–vector interaction using the N/D method and dispersion relations, which concludes that, while, for $J = 0$, one finds bound states, in the case of $J = 2$, where the interaction is also attractive and much stronger, no bound state is found. In that work, approximations are done for N and D and a subtracted dispersion relation for D is used, with subtractions made up to a polynomial of second degree in $s - s_{\text{th}}$, matching the expression to $1 - VG$ at threshold. We study this in detail for the $\rho\rho$ interaction and to see the convergence of the method we make an extra subtraction matching $1 - VG$ at threshold up to $(s - s_{\text{th}})^3$. We show that the method cannot be used to extrapolate the results down to 1270 MeV where the $f_2(1270)$ resonance appears, due to the artificial singularity stemming from the “on-shell” factorization of the ρ exchange potential. In addition, we explore the same method but folding this interaction with the mass distribution of the ρ , and we show that the singularity disappears and the method allows one to extrapolate to low energies, where both the $(s - s_{\text{th}})^2$ and $(s - s_{\text{th}})^3$ expansions lead to a zero of $\text{Re } D(s)$, at about the same energy where a realistic approach produces a bound state. Even then, the method generates a large $\text{Im } D(s)$ that we discuss is unphysical.
.....

Subject Index B60

1. Introduction

In Ref. [1], the chiral unitary approach for pseudoscalar mesons was extended to the interaction of vector mesons, concretely the $\rho\rho$ interaction, using the Bethe–Salpeter equation,

$$T = \frac{V}{1 - VG}, \quad (1)$$

where G is the loop function of the two ρ meson propagator and V the potential, obtained from the local hidden gauge Lagrangians [2–4], which contains a contact term and the ρ exchange term as shown in Fig. 1.

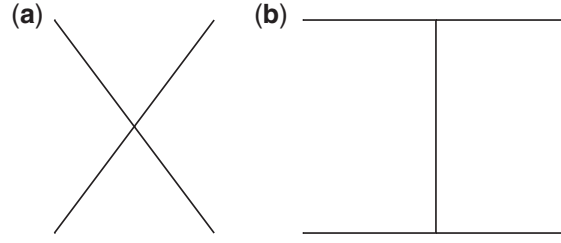


Fig. 1. Terms in the $\rho\rho$ interaction: (a) contact term; (b) ρ exchange term.

The potential V corresponding to these diagrams for $J = 2$ is

$$V = V_c + V_{\text{ex}}$$

$$V_c = -4g^2; \quad V_{\text{ex}} = -8g^2 \frac{3s - 4m_\rho^2}{4m_\rho^2}, \quad (2)$$

where $g = m_\rho/(2f_\pi)$ ($f_\pi = 93$ MeV). In Ref. [1], an approximation was made, where in the exchange of the ρ meson, the q^2 term in the propagator of the exchanged ρ , $[q^2 - m_\rho^2]^{-1}$, was dropped. This is actually what is done to establish the link between the local hidden gauge approach, with the exchange of vector mesons, and the chiral Lagrangians. The latter are obtained from the former neglecting q^2 in the propagator of the exchanged vector mesons.

Two dynamically generated resonances were found in isospin $I = 0$, one with total angular momentum $J = 0$, which could be related to the $f_0(1370)$, and the other with $J = 2$, which was associated to the $f_2(1270)$. The approach was generalized to SU(3) in Ref. [5], where other resonances like the $f_0(1710)$ and the $f_2'(1525)$ were also obtained.

In Ref. [6], the method used in Ref. [1] was questioned in relation to an improved relativistic vertex and keeping the q^2 dependence of the exchanged ρ propagator. Equation (1) was used in the on-shell factorization of the potential taking the ρ exchange term with the external legs on shell ($p_i^2 = m_\rho^2$). However, the method developed pathologies since the factorized on-shell ρ exchange term has singularities below threshold, giving rise to an unphysical infinity in the potential, and an imaginary part that also has a discontinuity. The method was discussed in Ref. [7] and it was shown to provide similar results to Ref. [1] close to threshold, but to be unsuited for the study of more bound states, as the $f_2(1270)$, because the unphysical singularity of the on-shell potential appeared around the energy of that state. In fact, the conclusion of Ref. [6] was that the $f_2(1270)$ was not obtained in that approach and was ruled out as a dynamically generated state from the $\rho\rho$ interaction. This conclusion is surprising because the $f_0(1370)$ appears bound in Refs. [1] and [6], and the potential for $J = 2$ is attractive and even more than twice as large as for $J = 0$ in the whole relevant energy range. According to the basic rules of quantum mechanics, if we find a bound state with a given potential, another potential with the same range and bigger attractive strength gives rise to a state that is more bound.

Concerning the total angular momentum of the two states, we should note that while the general rule in quantum mechanics is that states with higher L are less bound, because of the centrifugal potential in spherical coordinates, in the present case we have $J = 2$ and $J = 0$, but both with s-wave, coming from a different combination of spins of the two vectors, and it is the peculiar dynamics of the meson exchange that makes the $J = 2$ case more bound.

The effective range approach, which can give different results for $J = 0$ and $J = 2$, was invoked as a possible explanation for this feature in Ref. [6] and more recently in Ref. [8]. However, this argument cannot invalidate the quantum mechanics rule. Indeed, if the effective range formula fails to give a bound state in the case of the more bound potential, the only conclusion that one can draw is that the effective range formula,

$$T \sim \frac{-8\pi\sqrt{s}}{\frac{-1}{a} + \frac{1}{2}r_0p^2 - ip}, \quad (3)$$

cannot be extrapolated to the low energies where the bound state will appear.

In Ref. [7] it was shown that the singularity and imaginary parts that appear implicitly in the loops of the Bethe–Salpeter equation when the on-shell factorization is done were artificial, because the loop, evaluated exactly in Ref. [7], did not develop any singularity nor had an imaginary part below threshold. Instead, a method was proposed that kept the q^2 dependence of the ρ exchanged propagator in the loops and gave rise unavoidably to a bound state both in $J = 0$ and $J = 2$.

To the end of Ref. [6] a different method was proposed based on the N/D method, but, however, solved perturbatively. This method has been recently used in Ref. [8] and extended to SU(3) to match the results obtained in Ref. [5], with the conclusion that, while the method provides very similar results to Ref. [5] for small binding energies, it does not provide bound states in $J = 2$, as the $f_2(1270)$ and $f_2'(1525)$. The purpose of the present paper is to show in detail why and how this perturbative N/D method fails when one goes to large binding energies. Actually the authors of Ref. [8] seem to be aware of the problem since they say, “To investigate quantitatively possible poles beyond the near-threshold region, a more rigorous and complete treatment of the left-hand cuts is required”. However, even then, they conclude the absence of the $f_2(1270)$ and $f_2'(1525)$ as dynamically generated resonances.

2. Brief description of the method of Ref. [7]

In Ref. [6], the propagator of the exchanged ρ meson was projected in an s-wave:

$$D_\rho(p) = \frac{1}{p^2 - m_\rho^2 + i\epsilon} \xrightarrow{\text{s-wave}} -\frac{1}{4p^2} \text{Log} \left(\frac{4p^2 + m_\rho^2}{m_\rho^2} + i\epsilon \right) \equiv D_\rho^{(\text{s.w.})} \quad (4)$$

with $p^2 = s/4 - m_\rho^2$, on shell, and (s.w.) denotes s-wave. This on-shell factorized propagator becomes infinite at $s = 3m_\rho^2$ and for $s < 3m_\rho^2$, $D_\rho^{(\text{s.w.})}$ develops an imaginary part. In Ref. [7] it was shown that the use of Eq. (4), together with Eq. (1), leads to loop integrals below threshold that become infinite and have an imaginary part. This evidences the deficiencies of the method, since the one-loop terms can be evaluated exactly, as was done in Ref. [7]. The results are finite and have no imaginary part below threshold. These loop diagrams are shown in Fig. 2, and the momenta of diagram (b) are specified as in Fig. 3. The t -matrix for the diagram of Fig. 2(b) after performing analytically the q^0 integral can be written as

$$t(s) = \int \frac{d^3q}{(2\pi)^3} \frac{1}{2\omega(q)^2} \frac{1}{2\omega(\vec{p} - \vec{q})} \frac{1}{P^0 - 2\omega(q) + i\epsilon} \\ \times \frac{1}{\frac{P^0}{2} - \omega(q) - \omega(p - q) + i\epsilon} t_c(-m_\rho^2) V_{\text{ex}} V_c. \quad (5)$$

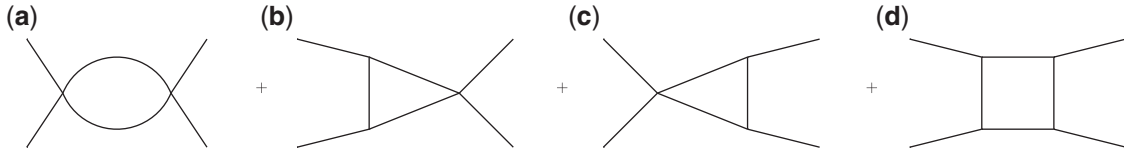


Fig. 2. Diagrams appearing at the one-loop level with the contact and ρ exchange terms.

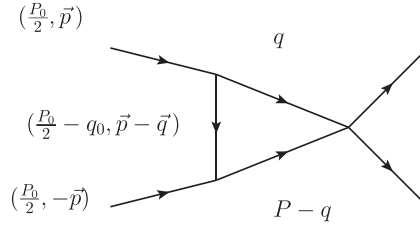


Fig. 3. Diagram of Fig. 2(b) showing explicitly the momenta of the particles.

In Eq. (5) one has approximated the ρ meson propagators with q and $P - q$ momenta in Fig. 3 by their positive energy part, since they are placed close to on shell in the loop, while for the exchanged ρ with momentum $(P^0/2 - q^0, \vec{P} - \vec{q})$, the full ρ propagator was kept. For the external \vec{P} momentum, we take an average of the momentum for the wave function that the approach generates. The results are smoothly dependent on this value [7]. Next one defines an effective ρ meson exchanged propagator $D_{\rho,\text{eff}}$ such that

$$(-m_\rho^2)V_{\text{ex}}V_cD_{\rho,\text{eff}}(s)G(s) = t(s), \quad (6)$$

with $G(s)$ the ordinary loop function that we regularize with the cut-off method:

$$G = \int_{|\vec{q}| \leq q_{\text{max}}} \frac{d^3q}{(2\pi)^3} \frac{\omega_1 + \omega_2}{2\omega_1\omega_2[(P^0)^2 - (\omega_1 + \omega_2)^2 + i\epsilon]}, \quad (7)$$

where q_{max} stands for the cut-off, $(P^0)^2 = s$, and $\omega = \sqrt{\vec{q}^2 + m_\rho^2}$. Then we define

$$\tilde{V}_{\text{ex}} = (-m_\rho^2)V_{\text{ex}}D_{\rho,\text{eff}} \quad (8)$$

and by construction we have

$$\tilde{V}_{\text{ex}}V_cG(s) = t(s). \quad (9)$$

With this \tilde{V}_{ex} we define the whole effective potential as

$$V_{\text{eff}} = V_c + \tilde{V}_{\text{ex}} \quad (10)$$

and if we do now

$$V_{\text{eff}}^2 G(s) = (V_c + \tilde{V}_{\text{ex}})^2 G(s) \quad (11)$$

we are summing exactly the diagrams of Figs. 2(a), (b), and (c), while providing an approximation for the diagram of Fig. 2(d). In Ref. [7] the diagram of Fig. 2(d) was also evaluated exactly and it was found that the approximation provided by Eq. (11), $\tilde{V}_{\text{ex}}^2 G(s)$, differed from the exact result by 10% around threshold and 18% at $\sqrt{s} = 1270$ MeV. Yet, taking into account the weight of all terms in Fig. 2, Eq. (11), and the sum of the exact expressions for them, differed by 4.5% at $\sqrt{s} = 1270$ MeV and by 2.5% at the $\rho\rho$ threshold. Then, V_{eff} was taken as an effective potential, and by means of

$$T = [1 - V_{\text{eff}} G]^{-1} V_{\text{eff}}, \quad (12)$$

we could find poles for $J = 0$ and $J = 2$, similar to those found in Ref. [1].

In order to take into account the ρ mass distribution in Ref. [7] one has to take the function G convoluted with the ρ spectral function as

$$\begin{aligned} \tilde{G}(s) = & \frac{1}{N^2} \int_{(M_\rho - 2\Gamma_\rho)^2}^{(M_\rho + 2\Gamma_\rho)^2} d\tilde{m}_1^2 \left(-\frac{1}{\pi} \right) \text{Im} \frac{1}{\tilde{m}_1^2 - M_\rho^2 + i\Gamma \tilde{m}_1} \\ & \times \int_{(M_\rho - 2\Gamma_\rho)^2}^{(M_\rho + 2\Gamma_\rho)^2} d\tilde{m}_2^2 \left(-\frac{1}{\pi} \right) \text{Im} \frac{1}{\tilde{m}_2^2 - M_\rho^2 + i\Gamma \tilde{m}_2} G(s, \tilde{m}_1^2, \tilde{m}_2^2), \end{aligned} \quad (13)$$

with

$$N = \int_{(M_\rho - 2\Gamma_\rho)^2}^{(M_\rho + 2\Gamma_\rho)^2} d\tilde{m}_1^2 \left(-\frac{1}{\pi} \right) \text{Im} \frac{1}{\tilde{m}_1^2 - M_\rho^2 + i\Gamma \tilde{m}_1}, \quad (14)$$

where $M_\rho = 770$ MeV, $\Gamma_\rho = 146.2$ MeV and for $\Gamma \equiv \Gamma(\tilde{m})$ we take the ρ width for the decay into two pions in a p-wave:

$$\Gamma(\tilde{m}) = \Gamma_\rho \left(\frac{\tilde{m}^2 - 4m_\pi^2}{M_\rho^2 - 4m_\pi^2} \right)^{3/2} \theta(\tilde{m} - 2m_\pi). \quad (15)$$

Actually, it was found in Ref. [7], that if the ρ meson exchange potential given by the propagator of Eq. (4) is convoluted by the ρ meson spectral function, it gives rise to a real part of the potential very similar to the one of Ref. [1]. The infinity of the real part disappears but the imaginary part remains although with no discontinuity. Taking into account the convolution of Eq. (13) makes the problem more realistic, since now there are components of the $\rho\rho$ system that are actually not so bound even for the $f_2(1270)$.

3. N/D approach of Ref. [8]

Here we briefly comment on the N/D method used in Ref. [8]. In the approach, the scattering amplitude is given by

$$T = N(s)D^{-1}(s) \quad (16)$$

with

$$N(s) = \sum_{m=0}^{n-1} \bar{a}'_m s^m + \frac{(s - s_0)^n}{\pi} \int_{-\infty}^{s_{\text{left}}} ds' \frac{\text{Im} T(s') D(s')}{(s' - s_0)^n (s' - s)},$$

$$D(s) = \sum_{m=0}^{n-1} \bar{a}_m s^m + \frac{(s-s_0)^n}{\pi} \int_{s_{\text{th}}}^{\infty} ds' \frac{\rho(s') N(s')}{(s'-s)(s'-s_0)^n}. \quad (17)$$

Given the extreme difficulty of the exact solution, a perturbative approach is used in Ref. [8] approximating $N(s)$ by the potential $V(s)$, such that, for one channel, one has

$$\begin{aligned} N(s) &= V(s); \\ D_2(s) &= \gamma_0 + \gamma_1(s-s_{\text{th}}) + \frac{1}{2}\gamma_2(s-s_{\text{th}})^2 \\ &\quad + \frac{(s-s_{\text{th}})s^2}{\pi} \int_{s_{\text{th}}}^{\infty} ds' \frac{\rho(s') V(s')}{(s'-s_{\text{th}}-i\epsilon)(s'-s-i\epsilon)s'^2}, \end{aligned} \quad (18)$$

with

$$\rho(s) = \frac{\sigma(s)}{16\pi s}; \quad \sigma(s) = 2p\sqrt{s} = \sqrt{(s-s_{\text{th}})s}, \quad (19)$$

where, in the last step, we have used that $m_1 = m_2 (= m_\rho)$ in the $\rho\rho$ channel, with p being the c.m. three momentum.

The parameters $\gamma_0, \gamma_1, \gamma_2$ in Eq. (18) are obtained matching $D_2(s)$ to $1 - VG$ of Eq. (1) around the $\rho\rho$ threshold, or equivalently, matching

$$P_2(s) \equiv \gamma_0 + \gamma_1(s-s_{\text{th}}) + \frac{1}{2}\gamma_2(s-s_{\text{th}})^2 \quad (20)$$

to

$$\omega_2(s) = 1 - V(s)G(s) - \frac{(s-s_{\text{th}})s^2}{\pi} \int_{s_{\text{th}}}^{\infty} ds' \frac{\rho(s') V(s')}{(s'-s_{\text{th}}-i\epsilon)(s'-s-i\epsilon)s'^2} \quad (21)$$

and then

$$\begin{aligned} \gamma_0 &= \omega_2(s_{\text{th}}); & \gamma_1 &= \omega_2'(s_{\text{th}}); \\ \gamma_2 &= \omega_2''(s_{\text{th}}). \end{aligned} \quad (22)$$

It is interesting to note that both $G(s)$ and the integral in Eq. (21) have a discontinuity of the derivative at threshold. However, the sum of the terms on the right-hand side of Eq. (21) is well behaved, as we show in the appendix. Yet, a high accuracy in the numerical integrals is needed to accomplish it. We use Gauss integration with a sufficient number of points to observe numerically the cancellation of the singular parts.

The final thing that we want to show is that since $N(s)$ has been taken as $V(s)$, in the approach of Ref. [8], where $D_\rho^{(s.w.)}$ of Eq. (4) is used for the ρ meson exchange potential, the T -matrix has unphysical singularities and an imaginary part around $s = 3m_\rho^2$. Hence, the method does not provide a realistic t -matrix. Yet, in Ref. [8], the zeros of $D(s)$ are used to determine whether the system has a pole or not, and $D(s)$ is a well behaved function since $V(s')$ is only used for $s' > s_{\text{th}}$ and is never extrapolated to their unphysical region. Then it is interesting to see what happens.

In order to understand the method and what it really accomplishes, we extend it to $(s - s_{\text{th}})^3$ and compare the results with those at order $(s - s_{\text{th}})^2$.

4. Derivation of $D(s)$ at $\mathcal{O}((s - s_{\text{th}})^3)$

In what follows we will compare the approximation of Eq. (18) for $D(s)$ to the exact value of $1 - VG$. But before that, we address the problem of extending Eq. (18) by making an extra subtraction and matching $1 - VG$ up to $(s - s_{\text{th}})^3$.

Equation (18) contains one subtraction at threshold and two subtractions at $s = 0$ to avoid problems with multiple subtractions at $s = s_{\text{th}}$. Yet, the matching to $1 - VG$ is done at threshold by means of Eqs. (20), (21), and (22)¹. We now make one extra subtraction of the integral of Eq. (18) at $s = 0$ and we obtain

$$D_3(s) = \gamma_0 + \gamma_1(s - s_{\text{th}}) + \frac{1}{2}\gamma_2(s - s_{\text{th}})^2 + \frac{1}{3!}\gamma_3(s - s_{\text{th}})^3 + \frac{(s - s_{\text{th}})s^3}{\pi} \int_{s_{\text{th}}}^{\infty} ds' \frac{\rho(s')V(s')}{(s' - s_{\text{th}} - i\epsilon)(s' - s - i\epsilon)s'^3}. \quad (23)$$

To obtain the γ_i coefficients we proceed as before and match

$$P_3(s) \equiv \gamma_0 + \gamma_1(s - s_{\text{th}}) + \frac{1}{2}\gamma_2(s - s_{\text{th}})^2 + \frac{1}{3!}\gamma_3(s - s_{\text{th}})^3 \quad (24)$$

to

$$\omega_3(s) = 1 - V(s)G(s) - \frac{(s - s_{\text{th}})s^3}{\pi} \int_{s_{\text{th}}}^{\infty} ds' \frac{\rho(s')V(s')}{(s' - s_{\text{th}} - i\epsilon)(s' - s - i\epsilon)s'^3} \quad (25)$$

around the $\rho\rho$ threshold, and then

$$\begin{aligned} \gamma_0 &= \omega_3(s_{\text{th}}); & \gamma_1 &= \omega_3'(s_{\text{th}}); \\ \gamma_2 &= \omega_3''(s_{\text{th}}); & \gamma_3 &= \omega_3'''(s_{\text{th}}). \end{aligned} \quad (26)$$

5. Wave function

The wave function in momenta space reads [9]

$$\langle \vec{p} | \psi \rangle = A \frac{\Theta(p_{\text{max}} - |\vec{p}|)}{E - \omega_1(p) - \omega_2(p) + i\epsilon}, \quad (27)$$

where $\omega_{1,2}(p) = \sqrt{\vec{p}^2 + m_{1,2}^2}$, and the normalization constant A for a bound state can be obtained through the condition $A^2 \int d^3p |\langle p | \phi \rangle|^2 = 1$, as

$$A = \sqrt{\frac{1}{\int_{p < p_{\text{max}}} d^3p \left| \frac{1}{E - \omega_1 - \omega_2} \right|^2}}, \quad (28)$$

while in coordinate space, throughout the Fourier transform, we have,

$$\langle \vec{r} | \psi \rangle = A \int_{p < p_{\text{max}}} \frac{d^3p}{(2\pi)^{\frac{3}{2}}} e^{i\vec{p} \cdot \vec{r}} \frac{1}{E - \omega_1(p) - \omega_2(p) + i\epsilon}. \quad (29)$$

¹ One can rearrange a polynomial of order s^3 in s in terms of a polynomial in $(s - s_{\text{th}})$ up to order $(s - s_{\text{th}})^3$.

Since the exponential part can be decomposed in terms of the spherical harmonic and Bessel functions,

$$e^{i\vec{p}\cdot\vec{r}} = 4\pi \sum_l i^l j_l(pr) \sum_m (-1)^m Y_{lm}(\theta_{\vec{r}}, \phi) Y_{l,-m}(\theta_{\vec{p}}, \phi), \quad (30)$$

one can write down the wave function in coordinate space as

$$\langle \vec{r} | \psi \rangle = A \int_{p < p_{\max}} p^2 dp 4\pi j_0(pr) \frac{1}{E - \omega_1(p) - \omega_2(p) + i\epsilon}, \quad (31)$$

with $j_0(pr) = \frac{\sin(pr)}{pr}$. In the above relation, the condition $\int Y_{00}(\theta_{\vec{p}}, \phi) Y_{0m}^*(\theta_{\vec{p}}, \phi) d\Omega_{\vec{p}} = \delta_{m0}$ was used. For the case of the $f_0(1370)$ and $f_2(1270)$, one needs to take into account the decay width of the ρ meson. This can be done by convoluting the wave function with the ρ meson mass distribution, like

$$\begin{aligned} \widetilde{\langle \vec{r} | \psi \rangle} &= \frac{1}{N^2} \int_{(M_\rho - 2\Gamma_\rho)^2}^{(M_\rho + 2\Gamma_\rho)^2} d\tilde{m}_1^2 \left(-\frac{1}{\pi} \right) \mathcal{I}m \frac{1}{\tilde{m}_1^2 - M_\rho^2 + i\Gamma\tilde{m}_1} \\ &\times \int_{(M_\rho - 2\Gamma_\rho)^2}^{(M_\rho + 2\Gamma_\rho)^2} d\tilde{m}_2^2 \left(-\frac{1}{\pi} \right) \mathcal{I}m \frac{1}{\tilde{m}_2^2 - M_\rho^2 + i\Gamma\tilde{m}_2} \langle \vec{r} | \psi; \tilde{m}_1^2, \tilde{m}_2^2 \rangle, \end{aligned} \quad (32)$$

with the normalization of Eq. (14). For the case of open channels, as occurs when taking into account the decay of the ρ meson through the convolution of the wave function, where some $\rho\rho$ components are unbound, the wave function can become non-normalizable, and we take the same normalization as in the bound case of Eq. (28), which allows us to compare the wave function at small distances.

6. Results

Let us first study how the methods discussed previously work for the case of the singular potential, in which the projection over s-wave keeping the q^2 dependence of the ρ propagator of Eq. (4) is done, as used in Refs. [6] and [8]. For this purpose, we take the sum of the contact term and the exchange term of Eq. (2), but with V_{ex} substituted by V'_{ex} , given by

$$V'_{\text{ex}} = V_{\text{ex}}(-m_\rho^2) D_\rho^{(\text{s.w.})} \quad (33)$$

$$V' = V_c + V'_{\text{ex}}. \quad (34)$$

In Ref. [6] extra terms were taken for the 3ρ vertex, which are negligible at energies close to threshold but are more relevant for lower energies. Yet, as noted in Ref. [7], the potential of Eq. (34) is remarkably similar to the one of Ref. [6] shown in Fig. 4 of that work. In Fig. 4 we plot the results for $1 - V'G$ as a function of the total energy. We use $q_{\max} = 1000$ MeV in G , Eq. (7), here and in the following [1,7]. We see that a singularity appears around $E = 1335$ MeV, corresponding to $s = 3m_\rho^2$. Let us see what we obtain using D_2 and D_3 from Eqs. (18) and (23). This requires us to first evaluate the functions $\omega_2(s)$ and $\omega_3(s)$ of Eqs. (21) and (25). The parameters γ_i that appear in $P_{2(3)}$, Eqs. (20)

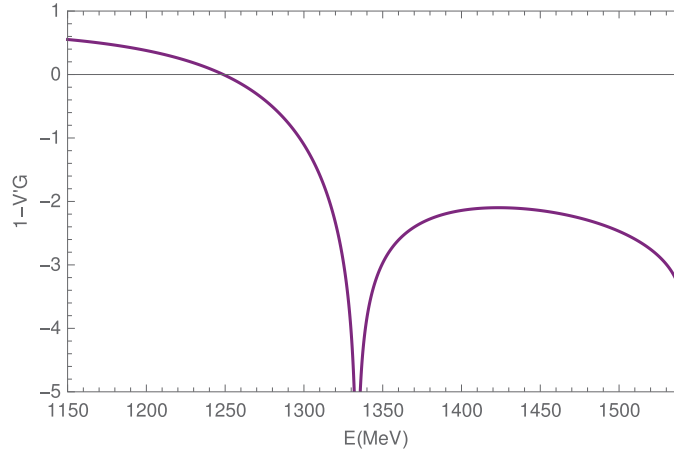


Fig. 4. The denominator of Eq. (1), $1 - V'G$, with the potential of Eq. (34), as a function of the energy.

and (24), are obtained from a fit of $\omega_{2(3)}$ to these polynomials for energies around the threshold in a range of 5(10) MeV. In Figs. 5 and 6, we plot ω_2 together with the approximation by the quadratic polynomial P_2 , and ω_3 with the cubic approximation, P_3 , respectively. The parameters γ_i are shown in Table 1. We can see that both ω_2 and ω_3 are well behaved at threshold and are smooth functions of the energy, and that in both cases we obtain a good fit to ω_2 and ω_3 by means of the polynomials P_2 and P_3 respectively, down to 1400 MeV. Note also that ω_2 and ω_3 are not equal, since the integrals in their expression are not the same, and neither are the polynomials P_2 and P_3 because two and three subtractions to the integrals, respectively, were done at $s = 0$, instead of the threshold. However, when we evaluate D_2 and D_3 , the two functions behave equally at threshold as a consequence of the fit that has been done to $1 - V'G$. This can be seen in Fig. 7, where we plot $1 - V'G$, D_2 , and D_3 . We can see that, indeed, both D_2 and D_3 are good approximations to $1 - V'G$. The approximation with D_2 is good down to 1450 MeV, while with D_3 the approximation improves and is good down to 1400 MeV. However, at energies around 1270 MeV, where the $f_2(1270)$ resonance should appear, the two approximations differ appreciably from each other, although neither of the two cuts the zero axis. This is essentially what is found in Ref. [8], and from where it is concluded that the $f_2(1270)$ is not dynamically generated from the $\rho\rho$ interaction. However, the exercise of the expansion to order $(s - s_{\text{th}})^3$ proves useful here. Indeed, what we see is that the approximation of D_3 tries to adjust better to $1 - V'G$ in the upper part of the energies before the singular point appears. This cannot be otherwise, since the D_2 , D_3 functions have been constructed precisely to avoid this singularity. There is no need to continue to higher orders in $(s - s_{\text{th}})$ because one can see what would happen. Indeed, higher orders would bend the curves more around 1350 MeV to adjust to $1 - V'G$ in that region and would lead to a curve that would be below D_3 . After many subtractions one would get close to the first branch of $1 - V'G$ before the singularity. Certainly, there is no convergence of the different orders in the region below the singularity and hence neither D_2 nor D_3 , nor any higher-order expansion, can be taken as a representation of a realistic D function below the singular peak. Thus, the claim that the $f_2(1270)$ does not appear from the $\rho\rho$ interaction based on the approach of Ref. [8] is not justified.

After this exercise, let us perform another one that is illustrative. A minimum requirement when one deals with unstable particles is to perform a folding of the magnitudes with the spectral function (mass distribution) of these particles. Following this philosophy, we fold the V' potential with the

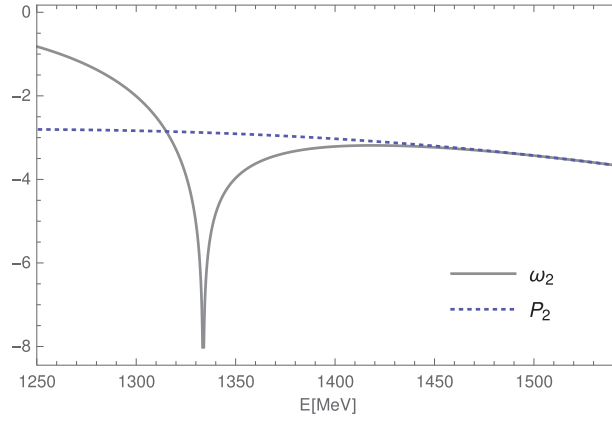


Fig. 5. The real part of the function ω_2 in comparison with P_2 , which appear in Eqs. (20), (21), and (22), with the potential V' .

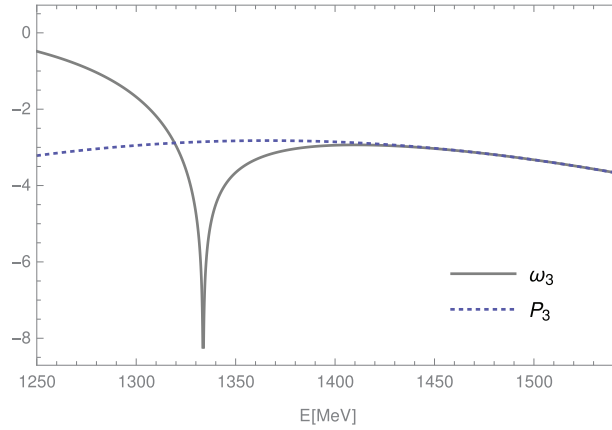


Fig. 6. The real part of the function ω_3 in comparison with P_3 from Eqs. (24), (25), and (26) with the potential V' .

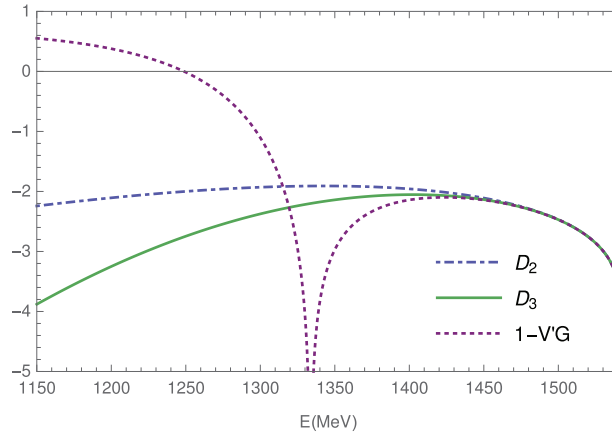


Fig. 7. The real part of the functions D_2 and D_3 from Eqs. (18) and (23) in comparison with $1 - V'G$.

ρ mass distribution using the same procedure as done to fold the G function in Eq. (13). This was done in Ref. [7] and found to provide a real part very similar to that of the potential used in Ref. [1]. There is still one objection to using this potential since the convolution spreads the imaginary part that V' artificially generates below threshold (see Fig. 5 of Ref. [7]). Indeed, as discussed in detail in Ref. [7], the loops evaluated using explicitly the full dynamics of the ρ exchange do not have

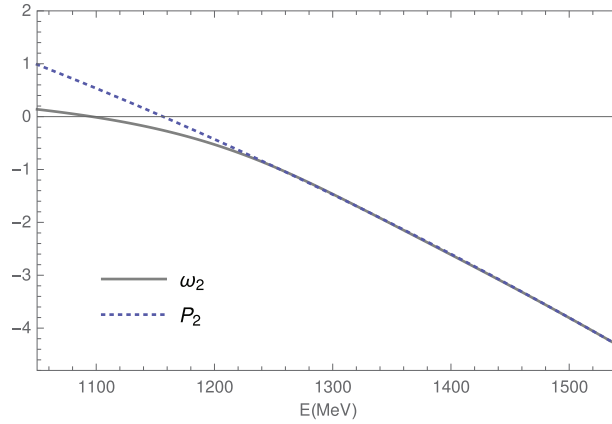


Fig. 8. The real part of the function ω_2 in comparison with P_2 , which appear in Eqs. (20), (21), and (22), with the convoluted potential V .

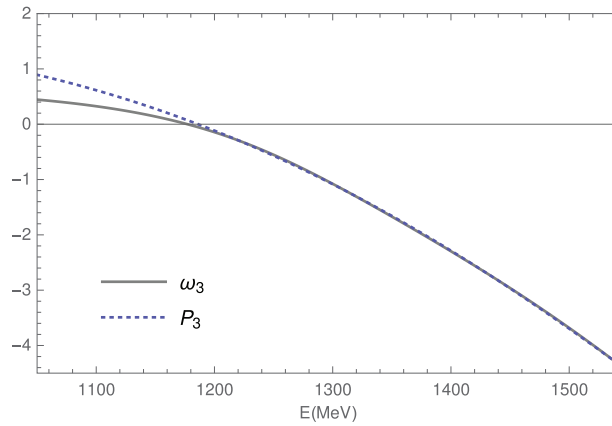


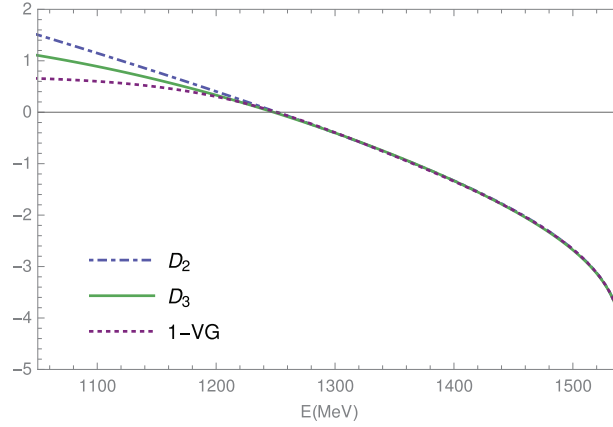
Fig. 9. The real part of the function ω_3 in comparison with P_3 from Eqs. (24), (25), and (26) with the convoluted potential V .

an imaginary part below threshold. This is because a) a bound state has a given energy and a wave function providing a distribution of real momenta, while the on-shell factorization gives imaginary momenta. In the bound state the particles are not on shell. b) In the loops of the diagrams of Fig. 2 the two intermediate ρ states in the s-channel can never be on shell if the external particles have an energy below threshold. As a consequence of that, and as was shown in Ref. [7], the exchanged ρ mesons do not develop a singularity and the diagrams do not give any imaginary part. However, since the real part is similar to that of the potentials used in Refs. [1] and [7], we perform the same exercise as before with this new potential, and the results are indicative of what one would get with the dispersion integral approach in all these other cases. The novelty of the convoluted potential is that the singularity disappears as soon as the convolution is done, as was shown in Ref. [7].

In Figs. 8 and 9, we again show ω_2 and P_2 for this new potential and ω_3 together with P_3 , respectively. The values of the γ_i parameters are shown in Table 1. As happened before using the same potential without convolution—see Figs. 5 and 6— ω_2 and ω_3 are well behaved below threshold, while P_2 and P_3 are very good approximations to ω_2 and ω_3 respectively. Next we plot $\text{Re } D_2$ and $\text{Re } D_3$, together with $\text{Re}(1 - VG)$, with V the convoluted potential, and show the results in Fig. 10. We can see now that both D_2 and D_3 are good approximations to $1 - VG$ down to energies of 1200 MeV. Moreover, in all these cases, the curves cut the zero axis around 1250 MeV, the region where

Table 1. Value of the γ parameters in Eqs. (18), (23) using the on-shell potential of Eq. (34) (upper two lines), and with the convolution of Eq. (13) (lower two lines).

Parameters	γ_0	$\gamma_1 \times 10^6 \text{ (MeV}^{-2}\text{)}$	$\gamma_2 \times 10^{12} \text{ (MeV}^{-4}\text{)}$	$\gamma_3 \times 10^{18} \text{ (MeV}^{-6}\text{)}$
D_2	-3.7	-2.0	-2.4	—
D_3	-3.7	-3.0	-3.9	7.7
D_2	-4.3	-4.1	0.04	—
D_3	-4.3	-5.1	-0.35	2.8

**Fig. 10.** The real part of the functions D_2 and D_3 from Eqs. (18) and (23) in comparison with the real part of $1 - V/G$, with V the convoluted potential.

the $f_2(1270)$ appears. This indicates that the dispersion approach provides a good convergence in a wide region of energies, provided that the potential is not singular. However, in the case of the singular potential, we showed above that the approach provides unrealistic results for energies below the singular point and should not be used.

In the case of the realistic V_{eff} potential evaluated in Ref. [7], it was constructed such that the exact loops are generated by means of $V_{\text{eff}}GV_{\text{eff}}$, as discussed in Sect. 2, and hence Eq. (12) provides a realistic approach to the scattering matrix and generates a bound state around 1270 MeV, as was shown in Ref. [7].

Finally, in Figs. 11 and 12, we provide the result for the wave functions in coordinate space of the $f_0(1370)$ and $f_2(1270)$ in the cases of a completely bound state and a $\rho\rho$ resonance, when the ρ meson is allowed to decay into two pions. We observe almost no difference if the convolution of the wave function is performed for the $f_2(1270)$, because of its larger binding energy, while for the $f_0(1370)$, the convolution has a bigger effect in the imaginary part of the wave function. For both resonances, the wave function for the s-wave shows a peak at $r = 0$. The probability density function, $4\pi r^2 |\psi|^2$, is depicted in Fig. 13, peaking around 0.5 fm. The oscillations in the wave function are caused by the sharp cut-off p_{max} around 1 GeV used². Because of the larger binding energy, these are restricted in space up to around 4–5 fm, where the wave function approaches a value near zero.

² We take $p_{\text{max}} = 1000$ MeV and 875 MeV for the $f_0(1370)$ and $f_2(1270)$ respectively [1].

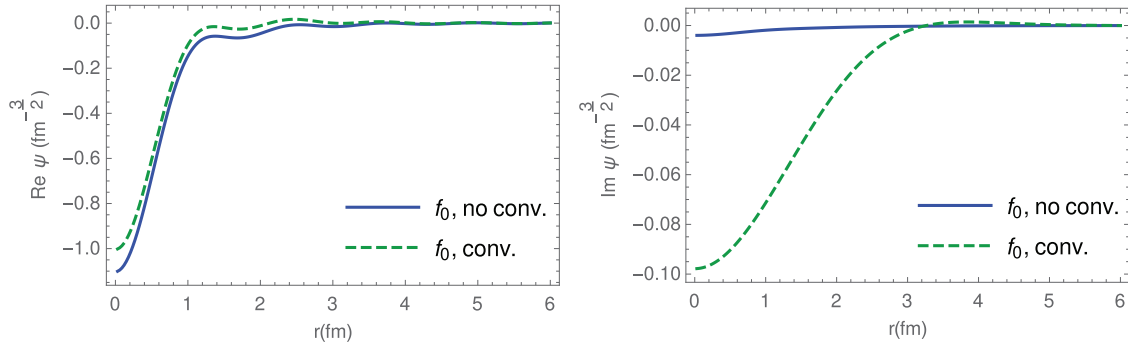


Fig. 11. Real and imaginary parts of the wave function in the coordinate space for the $f_0(1370)$, in the cases of no convolution and convolution with the ρ meson spectral function.

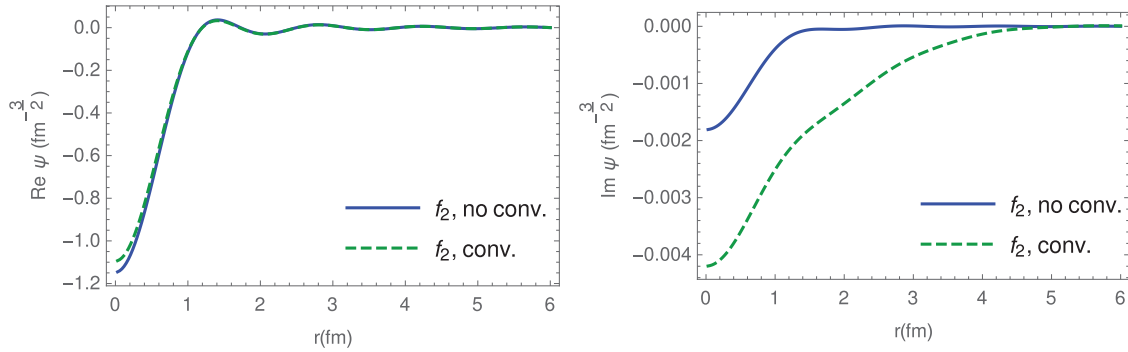


Fig. 12. Real and imaginary parts of the wave function in the coordinate space for the $f_2(1270)$, in the cases of no convolution and convolution with the ρ meson spectral function.

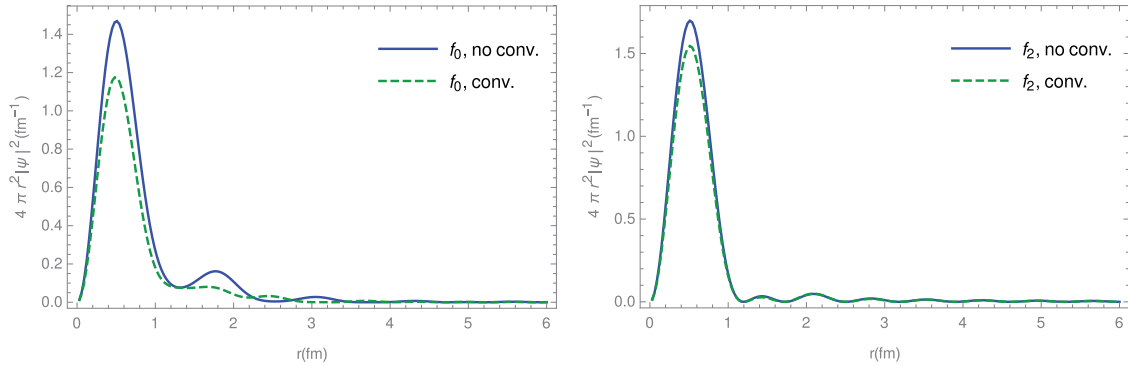


Fig. 13. Probability density distribution in the coordinate space for the $f_0(1370)$ (left) and $f_2(1270)$ (right), in the cases of no convolution and convolution with the ρ meson spectral function.

7. Conclusions

We have analyzed in detail the method proposed in Ref. [8] to find the poles of the vector–vector scattering amplitudes, specializing in $\rho\rho$ scattering. In order to avoid the use of an on-shell potential and the factorization in the Bethe–Salpeter equation proposed in Ref. [6], since that potential develops unphysical singularities, the authors of Ref. [8] proposed an approach based on the N/D method, performing some perturbative evaluation of $D(s)$, where the poles correspond to the zeros of $D(s)$. Apart from the approximation done to construct $D(s)$, an extra approximation is done to this $D(s)$

function performing subtractions and fitting the results to $1 - VG$ around threshold at order $(s - s_{\text{th}})^2$. In the present work we extended that approach to order $(s - s_{\text{th}})^3$ by doing an extra subtraction on the dispersion integral. This allowed us to better understand what the dispersion approach is accomplishing.

What we found is that, in spite of the fact that the dispersion relation was introduced to avoid the unphysical divergence of the on-shell ρ exchange potential, the new D function tries to adapt to $1 - V'G$ with the singular potential in the region before the singularity and cannot be used to extrapolate to the region below this energy where the $f_2(1270)$ state appears. On the other hand, we used a different potential, taking the same ρ exchange term but folding it with the ρ mass distribution. In this case the singularity disappears and the approach to $1 - VG$ by means of the D function of the dispersion relation is relatively good and can be extrapolated to relatively low energies. In this case we can see that $\text{Re}(1 - VG)$ and both $\text{Re} D_2$ and $\text{Re} D_3$ become zero at energies close to where the $f_2(1270)$ appears. However, V , D_2 , and D_3 , get unphysical imaginary parts. Yet, since $\text{Re} V$ is very similar to the effective potential used in Ref. [7], the exercise does tell us what to expect in those realistic cases.

In summary, the method proposed in Ref. [8] to avoid the pathologies of the use of the singular “on-shell” ρ exchange potential in Ref. [6] does indeed eliminate the artificial singularity of the $D(s)$ function found in Ref. [6], but we prove that its range of validity is constrained to energies much bigger than the one where the singularity appears and cannot be used to make predictions below this energy. But this is the case of the $f_2(1270)$ resonance that appears below that point.

On the other hand, our approach with V_{eff} , and $t = (1 - V_{\text{eff}}G)^{-1}V_{\text{eff}}$, with V_{eff} constructed as in Eq. (10), gives a pole corresponding to a bound state in $J = 2$, the $f_2(1270)$. This state is unavoidable based on basic quantum mechanics arguments since for $J = 0$, where the potential has about half the strength of $J = 2$, all the methods produce a bound state, and hence for an attractive potential with double strength a more bound state should be produced.

Acknowledgements

We thank F. K. Guo for useful comments. This work is partly supported by the DGICYT contract FIS2011-28853-C02-01, FEDER funds from the European Union, the Generalitat Valenciana in the program Prometeo, 2009/090, and the EU Integrated Infrastructure Initiative Hadron Physics 3 Project under Grant Agreement no. 283286. L.S.G. acknowledges support from the National Natural Science Foundation of China under Grant No. 11735003. R.M. acknowledges financial support from the Fundação de amparo à pesquisa do estado de São Paulo, FAPESP (Ref. 2017/02534-3), and the Talento program from the Community of Madrid (Ref. 2018-T1/TIC-11167).

Funding

Open Access funding: SCOAP³.

Appendix A. Cancellation of singularities in $\omega_2(s)$ and $\omega_3(s)$

We make the derivation for $\omega_2(s)$. The case of $\omega_3(s)$ is identical. In the definition of $\omega_2(s)$, Eq. (21), $G(s)$ has a discontinuity in the derivative at threshold, and also the integral appearing there. Here we show that in the difference of the two terms these singularities cancel and $\omega_2(s)$ is well behaved at threshold. Let us begin with the integral

$$I_2(s) = \frac{(s - s_{\text{th}})s^2}{\pi} \int_{s_{\text{th}}}^{\infty} ds' \frac{\rho(s')V(s')}{(s' - s_{\text{th}} - i\epsilon)(s' - s - i\epsilon)s'^2} \quad (\text{A.1})$$

with

$$\rho(s') = \frac{\sigma(s')}{16\pi s'}; \quad \sigma(s') = 2p\sqrt{s'} = \sqrt{(s' - s_{\text{th}})s'}, \quad (\text{A.2})$$

where p is the momentum of one ρ meson for the $\rho\rho$ system with energy $\sqrt{s'}$. It is convenient to work on the variable p :

$$\begin{aligned} 2\sqrt{p^2 + m_\rho^2} &= \sqrt{s'}; & p^2 + m_\rho^2 &= \frac{s'}{4}; & 2pd p &= \frac{ds'}{4}; \\ p &= \sqrt{\frac{s'}{4} - m_\rho^2} = \frac{1}{2}\sqrt{s' - s_{\text{th}}}. \end{aligned} \quad (\text{A.3})$$

Then, we have

$$I_2(s) = \frac{(s - s_{\text{th}})s^2}{\pi} \int_0^\infty \frac{dp p^2}{\pi \sqrt{s'} (s' - s_{\text{th}} - i\epsilon)(s' - s - i\epsilon)s'^2} V(s'). \quad (\text{A.4})$$

Note that p^2 in the numerator cancels $(s' - s_{\text{th}})$ in the denominator, showing that this denominator does not produce a singularity. Simplifying, we obtain

$$\begin{aligned} I_2(s) &= \frac{(s - s_{\text{th}})s^2}{(2\pi)^2} \int_0^\infty dp \frac{V(s')}{\sqrt{s'} (s' - s - i\epsilon)s'^2} \\ &= \frac{(s - s_{\text{th}})s^2}{(2\pi)^2} \int_0^\infty dp \frac{V(s')}{\sqrt{s'} (4p^2 + 4m_\rho^2 - s - i\epsilon)s'^2}. \end{aligned} \quad (\text{A.5})$$

On the other hand, $G(s)$ from Eq. (7) gives

$$G(s) = \int_0^{q_{\text{max}}} \frac{p^2 dp}{2\pi^2} \frac{1}{\omega(p)} \frac{1}{s - 4p^2 - 4m_\rho^2 + i\epsilon}. \quad (\text{A.6})$$

We can see that Eqs. (A.5) and (A.6) have the same singular denominator. We can write $I_2(s)$ as

$$I_2(s) = -\frac{(s - s_{\text{th}})s^2}{8\pi^2} \int_0^\infty \frac{dp}{\omega(p)} \frac{V(s')}{(s - 4p^2 - 4m_\rho^2 + i\epsilon)s'^2}. \quad (\text{A.7})$$

In order to see the singularity around threshold we can take $I_2(s)$ and $G(s)$ close to threshold and take $s^2/s'^2 \equiv 1$, since the singularity comes from $s' = s_{\text{th}}$. Thus, and just for values of s very close to threshold and small values of p in the integral,

$$\begin{aligned} 1 - VG(s) - I_2(s) &\simeq \\ 1 - \frac{V(s_{\text{th}})}{8\pi^2} \int \frac{dp}{\omega(p)} \frac{s - 4m_\rho^2 - 4p^2}{s - 4m_\rho^2 - 4p^2 + i\epsilon}, \end{aligned} \quad (\text{A.8})$$

and the singular denominator cancels with the numerator.

References

- [1] R. Molina, D. Nicmorus, and E. Oset, Phys. Rev. D **78**, 114018 (2008).
- [2] M. Bando, T. Kugo, S. Uehara, K. Yamawaki, and T. Yanagida, Phys. Rev. Lett. **54**, 1215 (1985).
- [3] M. Bando, T. Kugo, and K. Yamawaki, Phys. Rept. **164**, 217 (1988).

- [4] U.-G. Meissner, Phys. Rept. **161**, 213 (1988).
- [5] L. S. Geng and E. Oset, Phys. Rev. D **79**, 074009 (2009).
- [6] D. Gülmez, U.-G. Meißner, and J. A. Oller, Eur. Phys. J. C **77**, 460 (2017).
- [7] L.-S. Geng, R. Molina, and E. Oset, Chin. Phys. C **41**, 124101 (2017).
- [8] M.-L. Du, D. Gülmez, F.-K. Guo, U.-G. Meißner, and Q. Wang, Eur. Phys. J. C **78**, 988 (2018).
- [9] J. Yamagata-Sekihara, J. Nieves, and E. Oset, Phys. Rev. D **83**, 014003 (2011).